False alarm reduction in drilling process monitoring using virtual sample generation and qualitative trend analysis

Yupeng Li[a,b,c,d], Weihua Cao[a,b,c,*], R. Bhushan Gopaluni[d], Wenkai Hu[a,b,c], Liang Cao[d], Min Wu[a,b,c]

[a]*School of Automation, China University of Geosciences, Wuhan 430074, China*
[b]*Hubei key Laboratory of Advanced Control and Intelligent Automation for Complex Systems, Wuhan 430074, China*
[c]*Engineering Research Center of Intelligent Technology for Geo-Exploration, Ministry of Education, Wuhan 430074, China*
[d]*Department of Chemical and Biological Engineering, University of British Columbia, Vancouver, BC V6T 1Z3, Canada*

Abstract

Process monitoring is essential for ensuring the safety of geological drilling processes, but most existing monitoring systems suffer from false alarms. This study is motivated by the fact that many false alarms are generated from dynamic changes in signals under normal conditions. A new process monitoring method is proposed by analyzing the relationship between the input and output signals of a drilling normal behaviour model, enabling a fault detection decision by checking their qualitative trends at the change point. The main novelties of this study are: i) a data-driven normal behaviour model describing the fault-free operating condition is proposed to output expected healthy virtual samples; ii) a new alarm generation strategy is designed for reducing false alarms in drilling processes based on change point detection and qualitative trend analysis. Industrial case studies demonstrate the effectiveness and practicability of the method.

Keywords: Geological drilling process, virtual sample generation, change point detection, qualitative trend analysis,

1. Introduction

Geological drilling is a standard technology for exploring deeply buried resources. As drilling depth increases, the complex geological environment increases the formation uncertainty, making the drilling process more prone to unexpected faults. However, the harsh downhole environments such as high temperature, high pressure, and frequently changing operating states pose challenges to the timely and accurate detection of fault-related symptoms. Failure to detect these symptoms timely may result in serious accidents, such as blowouts and collapse. Thus, an effective drilling process monitoring system is urgently needed to prevent downhole accidents and reduce maintenance costs.

Demand for reducing non-production times has driven considerable attention toward developing advanced drilling process monitoring methods. Mathematical models describing drilling mechanisms are extensively studied in downhole fault diagnosis. A kick and loss incident detection method was proposed based on a single-phase hydraulic model of drilling fluid system using adaptive observers (Willersrud et al., 2015). By considering the gas characteristics in drilling fluid, a new integrated gas-liquid two-phase flow model was established for early kick detection (Yang et al., 2019). Towards detection of multiple downhole faults, an unscented Kalman filter-based ensemble classifier was utilized to classify faults based on the drilling fluid flow model (Jiang et al., 2020). In addition to drilling fluid-related faults, differential equation models describing the stick-slip and bit bounce faults were established in (Kamel and Yigit, 2014), and the corresponding stick-slip vibration suppression method was proposed using an event-triggered scheme (Lu et al., 2021). The main idea of the above mathematical model-based methods is to monitor the model parameter deviates from expected value or estimate the state of the system using state observers, thereby detecting downhole faults. An essential prerequisite for applying the method is an available accurate mechanism model. However, building such a model is costly since additional downhole instruments are required.

With the help of statistical and machine learning technologies, data-driven methods for ensuring process safety have been developed in recent years (Liu et al., 2022; Ji et al., 2019; Feng et al., 2019). A notable advantage of the machine learning technique is that only process data is required to create a model that can describe underlying relationships between various variables (Zhang et al., 2022). This provides an effective way for fault diagnosis in the era of big data. The data-driven methods are mainly based on continuous-valued process data, time series, and data distributions. An essential kick detection method is proposed to observe the changes in measurement signals, such as mass flow rate, pressure, and density (Nayeem

*Corresponding author at: School of Automation, China University of Geosciences, Wuhan 430074, China.

Email addresses: yupengli@cug.edu.cn (Yupeng Li), weihuacao@cug.edu.cn (Weihua Cao), bhushan.gopaluni@ubc.ca (R. Bhushan Gopaluni), wenkaihu@cug.edu.cn (Wenkai Hu), clubc19@mail.ubc.ca (Liang Cao), wumin@cug.edu.cn (Min Wu)

et al., 2016). Further, binary and multi-classifiers with drilling data as input were utilized to transform the fault diagnosis into a classification problem. For example, a lost circulation prediction model was developed based on a decision tree and neural networks using a large data set from 61 wells (Sabah et al., 2019). Time series analysis is an effective way to describe abnormal signal changes by extracting the change trend or direction caused by a fault. An improved piecewise approximation method was used for gas kick diagnosis via pattern recognition (Sun et al., 2018). An early warning model for screenout scenarios was developed by integrating the autoregressive moving average and locally weighted linear regression (Hu et al., 2020). There were a few diagnosis methods that analyze drilling time series using similarity measures, such as morphological distance (Zhao et al., 2019), local similarity (Zhang et al., 2021), and dynamic time warping (Li et al., 2021b). Then, the condition is determined by comparing the distance between the sample and fault templates. Data distribution organizes raw data into graphs, showing advantages in incipient anomaly detection (Chen et al., 2019; Zhang and Zhao, 2022). The dissimilarity of data distribution was exploited to detect bit bounce faults based on generalized Gaussian distribution (Li et al., 2021c). By combining divergence matrix and time series information, normal operation zones were established to detect drilling abnormalities (Li et al., 2021a). Although promising results were achieved using the distribution feature, these methods need to model multiple operating modes respectively and are prone to false alarms during the mode-shifting process.

The above studies provide effective solutions for drilling process monitoring and fault diagnosis. However, an easily overlooked practical problem is that formation uncertainties and operating state shifts often cause dynamic changes in signals and lead to false alarms. Frequent false alarms always impact the driller's decision-making and even reduce their trust in the alarm system. It is desirable to reduce false alarms by investigating the normal operational behaviour of the drilling process. For industrial processes with limited training data, virtual sample generation algorithms were proposed to generate samples similar to the training set (Zhu et al., 2021). The strategy to enhance drilling datasets using generative adversarial networks was demonstrated in (Wang et al., 2022). Inspired by this idea, it is possible to develop a reconstruction model that describes the expected behaviour of the process based on healthy data. Then, potential faults are detected by monitoring fault-sensitive signals for deviations from expected normal values.

This study focuses on drilling process monitoring and false alarm reduction. The critical point is to develop a drilling normal behaviour model whose input is real-time data, and the output is expected healthy data. Then, the fault detection decision is made based on the dissimilarity between the expected output and the input. Considering that the prediction model's performance is prone to downhole environments, the dissimilarity is calculated quantitatively rather than qualitatively. Specifically, the decision is made by checking the change direction of the expected output and the real-time signal. The main novelties of the proposed method are: 1) A drilling normal behaviour model is proposed to generate expected healthy virtual samples; 2) A new alarm generation strategy is designed for reducing false alarms in drilling processes using change point detection and qualitative trend analysis. The proposed method is only based on healthy data and does not require a faulty dataset.

This paper is organized as follows: Section 2 introduces the process monitoring problem to be solved. Section 3 shows the technical details of the proposed method. Section 4 presents case studies to illustrate the method's effectiveness. Section 5 gives some concluding remarks.

2. Problem formulation

The primary elements of a vertical spindle drilling system include the drilling rig, drill string, drill bit, hook, drilling fluid, mud pit, and mud pump (Li et al., 2021c; Zhou et al., 2022). The drill string is a hollow steel pipe extending from the surface to the bottom of the well. The drilling rig outputs a specific Torque (TRQ) to drive the drill string to rotate, where the rotational speed is expressed as Rotate Per Minutes (RPM). Meanwhile, the Weight On Bit (WOB), generated by part of the gravity of the drill string itself, is applied to the drill bit to break the rock. Another essential part of the drilling system is the drilling fluid, which is pumped through the drill string to the downhole drill bit and returned to the surface with broken cuttings. The drilling fluid improves drilling efficiency and wellbore stability. The Stand Pipe Pressure (SPP) measures the pressure consumed throughout the drilling fluid circulation.

Auxiliary monitoring systems equipped with current drilling systems ensure drilling safety by comparing process signals with their corresponding thresholds. It is difficult for such systems to cope with all the tricky scenarios in drilling processes. For example, Fig. 1 shows time series plots of RPM and TRQ under a faulty condition, where the three-sigma limits are used to monitor the process. The blank area indicates the fault-free state, and the green and red areas represent the periods corresponding to false alarms and actual faults, respectively. The drilling system faces the following two problems:

- The measured signal is subjective to stratigraphic uncertainty, in-hole noise, and various healthy drilling states, such as dynamic shifting between multiple operating states. These disturbances and dynamic processes are likely to cause drastic changes in signals.
- The driller is often plagued by frequent false alarms, which may cause unnecessary scrambling and prevent real alarms from being detected, thus leading to downhole incidents, such as lost circulation, kick, and stuck pipe.

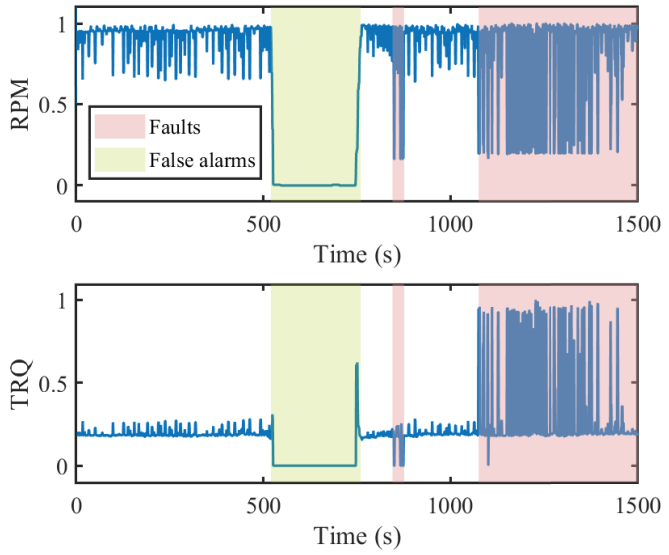

Figure 1: Time series plots of normalized RPM and TRQ signals under a faulty condition, where the blank area indicates the fault-free state, and the green and red ares represent the periods corresponding to false alarms and faults, respectively.

This work proposes a novel method to reduce false alarms in drilling processes to overcome the above practical problems. Given the drilling time series under normal conditions, the first step is to build a drilling normal behaviour model $\mathcal{M} : \boldsymbol{x} \rightarrow \boldsymbol{y}$, which can output the corresponding expected healthy sequence $\boldsymbol{y}$ with the real-time input sequence $\boldsymbol{x}$. The second step is to compare the dynamic trends of $\boldsymbol{x}$ and $\boldsymbol{y}$ to determine whether the drilling system deviates from the healthy state. For every single variable, the first-order trend information of $\boldsymbol{x}$ and $\boldsymbol{y}$ are extracted as z_x and z_y using the linear regression model with sliding windows. If either signal changes significantly, the qualitative trends d_x and d_y are extracted, and the fault detection decision is made by checking that d_x and d_y are consistent.

3. The proposed method

This section presents two main steps of the proposed drilling process monitoring method: establishment of the drilling normal behaviour model and change point detection via density-ratio estimation.

3.1. Establishment of the drilling normal behavior model

A well-trained drilling normal behaviour model can reconstruct the expected healthy data based on the current input. In the training process, the model should learn the characteristics of the process data under normal conditions. However, it is difficult to build such models using linear prediction methods due to nonlinear disturbances such as alternating between soft and hard formations, multiple operating states, and downhole measurement noise. Since the drilling operation is a continuous process, its health status is reflected by the temporal dependency of the drilling time series. Recently, studies found that the Long Short-Term Memory (LSTM) and gated recurrent units are useful in time series modeling tasks, and LSTMs perform better on larger datasets (Ni et al., 2022). Thus, the LSTM is used to describe complex nonlinear and sequence dependencies. Autoencoder (AE) is utilized to establish the drilling normal behaviour model.

AE is an unsupervised learning technique that learns a representation of a training dataset (LeCun, 1987). An AE is mainly composed of an encoder and a decoder, both of which are neural networks. The encoder η maps the drilling data into a hidden layer $\mathcal{H}$, and the decoder δ reconstructs the input data based on the information in the hidden layer.

In this study, the AE is utilized to establish the model that can reconstruct the drilling data under normal conditions. It is framed as a supervised learning problem tasked with outputting an expected healthy data $\mathcal{Y}$ corresponds to the input real-time collected data $\mathcal{X}$, such that:

$$\begin{aligned} \eta &: \mathcal{X} \rightarrow \mathcal{H} \\ \delta &: \mathcal{H} \rightarrow \mathcal{Y} \end{aligned}. \tag{1}$$

A simple feedforward neural network is a commonly used network architecture for η and δ. However, the feedforward neural network can hardly find the complex dependencies among drilling time series. Considering that the LSTM is designed to handle sequence dependence, it is incorporated into the structure of the AE (Chen et al., 2021; de Pater and Mitici, 2023). Here, the LSTM is utilized to build both η and δ models. The structure of the proposed drilling normal behaviour model based on LSTM-AE is displayed in Fig. 2. The input of the LSTM-encoder model is the time series of drilling signals, which are processed by three gates: an input gate i, a forget gate f, and an output gate o. The output is determined by both the input and the unit state related to previous samples.

Before feeding the raw drilling time series data into the LSTM-encoder model, all data were normalized and ranged between 0 and 1 to analyze different signals on equal footing. For each raw time series x^o, the normalized value at time k is

$$x(k) = \frac{x^o(k) - x^o_{min}}{x^o_{max} - x^o_{min}}, \tag{2}$$

where x^o_{min} and x^o_{max} represent the minimum and maximum values of x^o, respectively.

Then the normalized time series $x(k)$ and hidden state $s(k-1)$ are fed into the forget gate f, while the corresponding output is

$$f(k) = \psi(W_f[x(k), s(k-1)] + b_f), \tag{3}$$

where ψ denotes the sigmoid activation function, W_f represents the weights, and b_f indicates the biases. Similarly, W and b with subscripts in the following formulas repre-

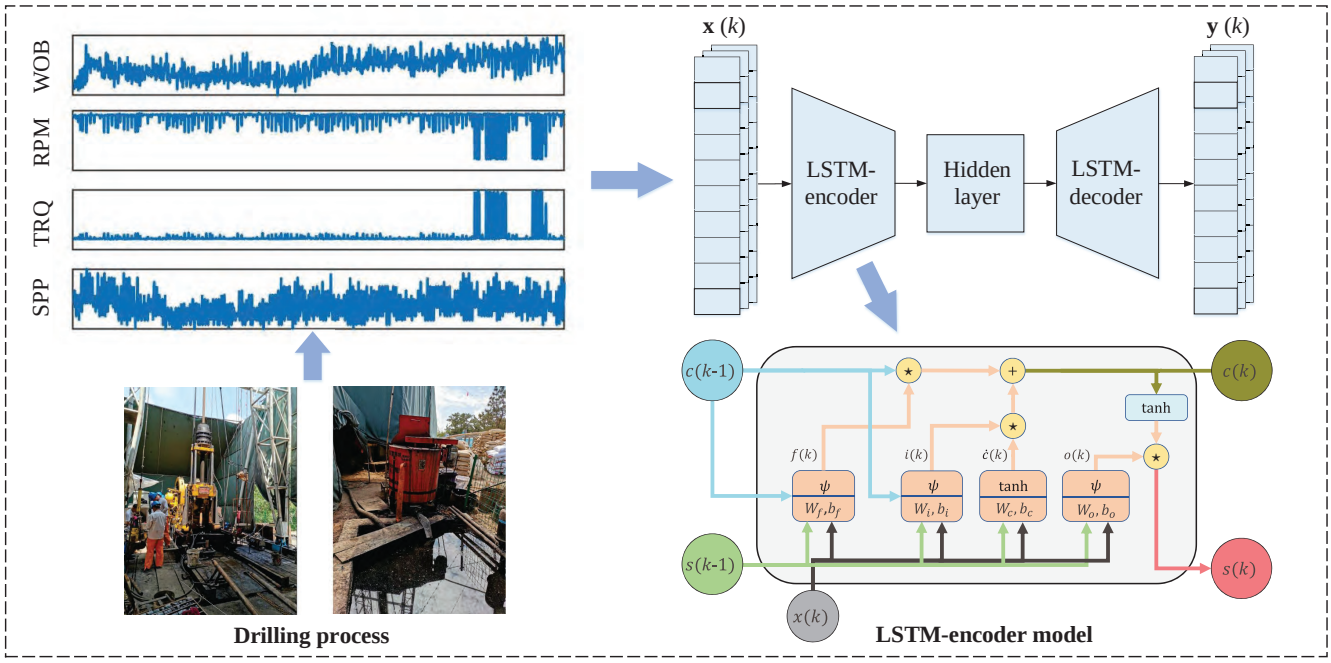

Figure 2: Structure of the drilling normal behaviour model based on LSTM-AE.

sent the weights and biases of different layers, respectively. Then, the forget gate abandons partially historical information to update the current hidden state $s(k)$.

The input gate i controls the information passed from $x(k)$ and $s(k-1)$ to the unit $c(k)$ as

$$i(k) = \psi\left(W_i[x(k), s(k-1)] + b_i\right). \tag{4}$$

In addition, the memory cell value $\dot{c}(k)$ is calculated as

$$\dot{c}(k) = \tanh\left(W_c[x(k), s(k-1)] + b_c\right). \tag{5}$$

Further, the unit $c(k-1)$ is updated based on $f(k)$ and $i(k)$ by the following formula:

$$c(k) = f(k) \star c(k-1) + i(k) \star \dot{c}(k), \tag{6}$$

where $\star$ represents the Hadamard product.

After updating the unit state, the value of the output gate $o(k)$ is updated as

$$o(k) = \psi(W_o(x(k), s(k-1)) + b_o). \tag{7}$$

Based on $o(k)$ and $c(k)$, the output of the LSTM-encoder δ is calculated, that is, the hidden layer sequence $s(k)$:

$$s(k) = o(k) \star \tanh(c(k)). \tag{8}$$

Similarly, the output of the LSTM-decoder is the reference sequence $y(k)$.

Based on healthy historical data, the normal behaviour model is trained by minimizing the distance between $\mathcal{X}$ and $\mathcal{Y}$. The distance is also known as the reconstruction error and is calculated as

$$\mathcal{L}(\mathcal{X} \,||\, \mathcal{Y}) = \arg\min_{\eta,\delta} \|\mathcal{Y} - \mathcal{X}\|^2. \tag{9}$$

Consequently, the trained η and δ can reconstruct the expected output $y(k)$ corresponding to each point $x(k)$ in the input sequence, enabling fault detection by comparing the reference output and real-time input.

3.2. Change point detection via density-ratio estimation

Decision-making of the drilling fault detection is realized by comparing the dynamic characteristics of the real-time signal and that of the reconstructed signal. According to Section 2, the dissimilarity is calculated qualitatively rather than quantitatively due to the stratigraphic uncertainty. Specifically, if either signal changes significantly, the downhole fault is detected by checking whether the qualitative trends of y and x are in the same direction.

Since the dynamic characteristics of the signal can be described by a linear model, the change detection is performed by detecting the change point of the first derivative signal rather than the original signal. Let $\{v(k)|v = x, y\}$ be an element of the drilling time series at k. The first derivative $z(k)$ of the input signal $v(t)$ over the period $[k-w+1, k]$ is estimated as

$$\hat{v}(t) = z(k)t + e(k), t \in [k-w+1, k], \tag{10}$$

where w denotes the sliding window length, the first derivative z and the intercept parameter e are calculat-

ed by minimizing the approximation errors, i.e.,

$$\min \sum_{t\in[k-w,k]} \left[v(t)-\hat{v}(t)\right]^2. \tag{11}$$

Now the problems to be solved are to detect the change points and extract the qualitative trend.

Some pioneering studies demonstrated that change detection in the time series could be realized by comparing the distribution of the samples collected online and that of a reference set (Brodsky and Darkhovsky, 1993). One critical step is to define the dissimilarity measure; the other is to obtain the distribution of the object data set. For instance, the Pearson (PE) divergence is a standard measure of the difference from distributions $P(A)$ to $P(B)$. However, drilling data distributions may not be accurately described using pre-defined parameters. Hence, this study exploits another divergence estimation approach based on density ratio. The main idea is to detect the change point by calculating the density-ratio function $\frac{P(A)}{P(B)}$ directly, without going through estimating the distributions $P(A)$ and $P(B)$ separately.

Assume that the probability distribution of the online first derivative z is denoted as $P(z)$, and the reference distribution under the normal condition is $P_r(z)$. The PE divergence from $P(z)$ to $P_r(z)$ is defined as:

$$\mathrm{PE}(P\|P_r)=\frac{1}{2}\int P_r(z)\left(\frac{P(z)}{P_r(z)}-1\right)^2 dz, \tag{12}$$

where the PE distance is non-negative and equals 0 only when $P(z)=P_r(z)$.

Although the analytic form of $P(z)$ and $P_r(z)$ are unknown, eq. (12) can be accurately solved by density-ratio estimation. Here, the Relative unconstrained Least-Squares Importance Fitting (RuLSIF) algorithm is utilized to estimate the density ratio analytically (Yamada et al., 2013). The RuLSIF defines the α-relative PE divergence as:

$$\begin{aligned}\mathrm{PE}_\alpha(P\|P_r)&=\mathrm{PE}(P\|g_\alpha)\\&=\frac{1}{2}\int P_r(z)\left(\frac{P(z)}{g_\alpha(z)}-1\right)^2 g_\alpha(z)dz,\end{aligned} \tag{13}$$

where $\alpha\in(0,1)$, and $g_\alpha(z)=\alpha P(z)+(1-\alpha)P_r(z)$. The α-relative density ratio is defined as:

$$r_\alpha(z)=\frac{P(z)}{g_\alpha(z)}. \tag{14}$$

It has been proved that $r_\alpha(z)$ is bounded by α^{-1} even if the density ratio is unbounded (Liu et al., 2013). The α-relative density ratio is modelled using the sum of serval kernel models as:

$$\hat{r}_\alpha(z)=h(z)=\sum_{i=1}^{n}\phi_i\mathcal{K}(z,z_i), \tag{15}$$

where n is the number of samples in a sliding window, $\phi=(\phi_1,...,\phi_n)$ are determined based on drilling samples, and $\mathcal{K}$ denotes the Gaussian kernel function as:

$$\mathcal{K}(z,z_i)=\exp\left(-\frac{\|z-z_i\|^2}{2\sigma^2}\right), \tag{16}$$

where σ represents the width of the kernel, which is determined using an empirical formula as (Gonzalez et al., 2015)

$$\sigma=\left(\frac{4s_z^5}{3n}\right)^{\frac{1}{5}}, \tag{17}$$

where s_z denotes the variance of z in the window.

With the kernel model $h(z)$ in eq. (15), the α-relative PE divergence between $P(z)$ and $P_r(z)$ is estimated only using the online segment $Z=[z(1),z(2),...,z(m)]$ and reference segment $Z^r=[z^r(1),z^r(2),...,z^r(\tilde{n})]$ as (Yamada et al., 2013)

$$\begin{aligned}\hat{\mathrm{PE}}_\alpha(P\|P_r)=&\frac{1}{2m}\sum_{j=1}^{m}\left(2\hat{h}(z_j)-\alpha\hat{h}(z_j)^2\right)\\&-\sum_{i=1}^{\tilde{n}}\frac{(1-\alpha)}{2\tilde{n}}\hat{h}(z_i^r)^2-\frac{1}{2}.\end{aligned} \tag{18}$$

where m and $\tilde{n}$ represent the number of samples in the online and reference segments, respectively. Compared to the asymmetric metric in eq. (18), a symmetric form shows better performance in change point detection (Liu et al., 2013). Here, the symmetrized form of the PE divergence

$$S_\alpha=\mathrm{PE}_\alpha(P\|P_r)+\mathrm{PE}_\alpha(P_r\|P) \tag{19}$$

is utilized to describe the difference between $P(z)$ and $P_r(z)$ to detect the change point.

Taking S_α as the change score, the change point detection problem is transformed into measuring whether the online S_α significantly deviates from a normal range. Thus, the threshold S_{th} is designed based on plenty of S_α samples under normal conditions.

Assuming S_α samples are Gaussian distributed, the S_{th} is determined based on the cumulative distribution function under a confidence level β, i.e.,

$$P(u\le S_{th})=\int_0^{S_{th}}\Gamma(u)du=\beta. \tag{20}$$

where $\Gamma(u)$ denotes the distribution of historical S_α samples under the normal condition.

In online monitoring, the change detection is formulated as the following hypothesis testing problem, i.e.,

$$\begin{cases} S_\alpha\le S_{th}: & z(k) \text{ is not a change point,}\\ S_\alpha> S_{th}: & z(k) \text{ is a change point.}\end{cases} \tag{21}$$

However, even if a change point is detected, it may not be caused by a downhole fault, so the trend of the change

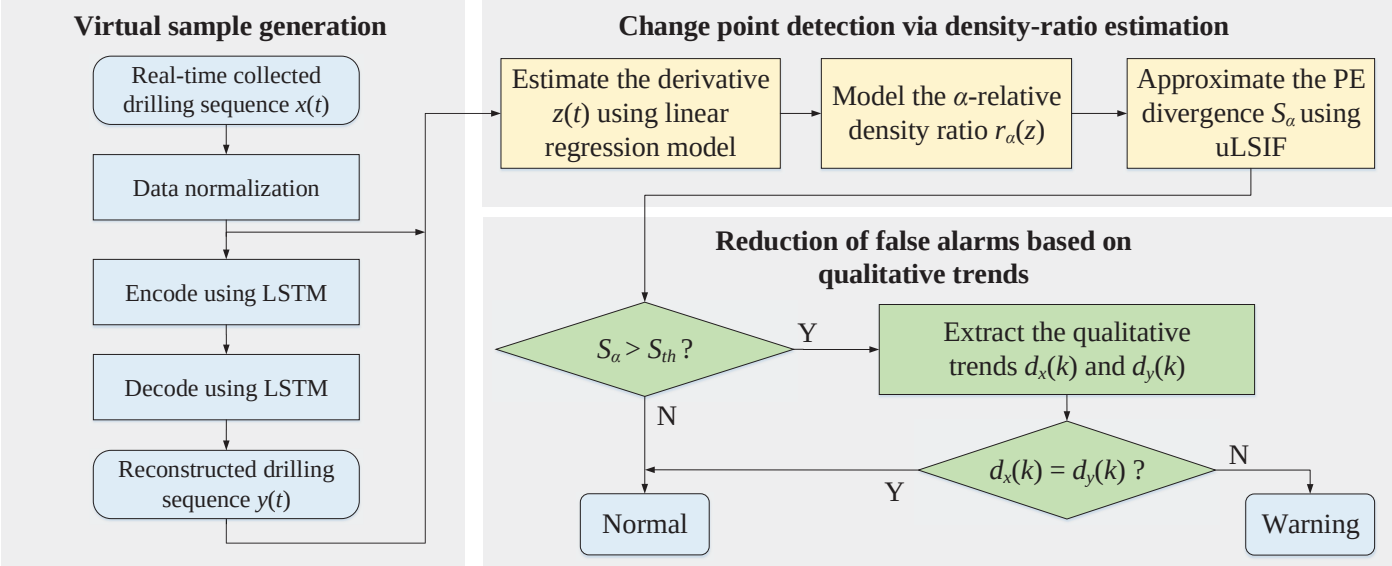

Figure 3: A framework of the drilling process monitoring method.

point needs to be extracted for further analysis.

Since the qualitative trend is more robust to downhole disturbance than the quantitative trend, the qualitative trend at the change point is extracted. If a change point is detected at k, the qualitative trend is defined as (Hu et al., 2022a)

$$d_v(k) = \begin{cases} 1: & \mu_k < \mu_n, \\ -1: & \mu_k > \mu_n, \end{cases} \tag{22}$$

where μ_k and μ_n denote the mean values of samples in the current window and normal historical data, respectively, and $d_v(k) = 0$ indicates no change point is detected. If the trend of the original signal $d_x(k)$ is consistent with that of the reconstructed signal $d_y(k)$, it implies that the system is in a normal condition; otherwise, there is a fault.

3.3. Process monitoring and false alarm reduction

The framework of the proposed method is shown in Fig. 3. The healthy historical data is normalized in the training phase to establish the drilling normal behaviour model based on the LSTM-AE structure in eq. (1). The alarm threshold S_{th} is determined using eq. (20) based on healthy data. The online fault detection mainly includes the following detailed steps:

- *Step 1:* The normalized real-time input sequence $x(t)$ is fed into the drilling normal behaviour model whose output is the reconstructed sequence $y(t)$;
- *Step 2:* Both $x(t)$ and $y(t)$ sequences are segmented by the sliding window, and then the corresponding first derivatives $z_x(t)$ and $z_y(t)$ are estimated respectively using the linear regression model in eq. (10);
- *Step 3:* The α-density ratio $r_\alpha(z)$ is calculated to detect changes in $z(t)$ based on PE divergence, and then $r_\alpha(z)$ is estimated using the kernel model in eq. (16);
- *Step 4:* The PE divergence S_α in eq. (19) is calculated as the change score; if the change score exceeds a pre-defined threshold S_{th}, treat it as a change point and further extract its qualitative trend $d(k)$ using eq. (22);
- *Step 5:* For each variable, check whether the qualitative trends $d_x(k)$ and $d_y(k)$ are consistent; if so, the system is normal; otherwise, it is a fault.

To evaluate the performance of the proposed process monitoring method, commonly used metrics, including False Alarm Rate (FAR), Missed Alarm Rate (MAR), and accuracy, are calculated as follows:

$$F_A = \frac{n_{\text{fn}}}{n_{\text{tp}} + n_{\text{fn}}} \times 100\%, \tag{23}$$

$$M_A = \frac{n_{\text{fp}}}{n_{\text{tn}} + n_{\text{fp}}} \times 100\%, \tag{24}$$

$$\text{Acc} = \frac{n_{\text{tp}} + n_{\text{tn}}}{n_{\text{fn}} + n_{\text{tn}} + n_{\text{fp}} + n_{\text{tp}}} \times 100\%, \tag{25}$$

where n_{fn} is the number of samples misclassified as faults under healthy conditions, n_{tp} denotes the number of samples correctly classified under healthy conditions, n_{fp} represents the number of faulty samples misclassified into normal, and n_{tn} stands for the number of faulty samples correctly classified under abnormal conditions.

4. Case studies

This section provides three industrial case studies with data from a geological drilling project in Shandong province, China, to illustrate the effectiveness of the proposed method. In this project, a drill operation cycle lasts about 1,000-3,000 seconds. The drilling normal behaviour model is established using 30,000 historical samples of RPM, TRQ, WOB, and SPP in the following three cases. The

training set consists of multiple non-adjacent segments collected from extensive historical data under normal drilling conditions. It is found through experiments that a shorter window is more sensitive to abnormal signal changes, while a longer window has a better noise suppression performance but a longer detection delay. The detection delay and sensitivity to abnormalities should be balanced in the change point detection. In view of the engineering expertise of operators, both the online segment m and the reference segment $\tilde{n}$ are composed of 60 samples. Analogously, the sliding window length for calculating the first derivative is 30 samples.

4.1. Case 1

In Case 1, the time series plots of the four original drilling process signals are shown in Fig. 4. The drilling system was in a steady state before $t = 500s$. Then, the drilling operator changed the set-point, and the system shifted to another operating state, causing step changes in the WOB, RPM, and TRQ signals. The system reverted to the previous steady state at $t = 750s$. Subsequently, the occurrence of downhole abnormalities caused significant fluctuations in RPM, TRQ, and SPP signals in $t \in [900, 950]$. As the drill bit encountered hard formations, RPM and TRQ changed drastically from $t = 1080s$ and lasted about 420 seconds. A stuck pipe fault caused the fluctuation of RPM and TRQ signals during this period.

With the input of the signals in Fig. 4, the proposed normal behaviour model is applied to calculate the corresponding reconstructed drilling signals shown in Fig. 5. Similar to the original signals, significant changes were detected in reconstructed signals in $t \in [550, 750]$, indicating that these changes were normal patterns learned from healthy historical data. Subsequently, all reconstructed signals returned to the steady-state at $t = 1080s$. This implies that drastic changes should not appear in original signals under normal conditions from $t = 1080s$.

Take the RPM signal as an example to illustrate the effect of the proposed method. Figs. 6 and 7 show the change detection results based on the original and the reconstructed RPM signals, respectively. To capture the dynamic features, the change detection is conducted based on the first derivative of the original signal. Figs. 6(a)-(c) show time series plots of the original RPM signal x, the PE divergence S_a of the first derivative z_x, and the corresponding qualitative trend d_x, respectively. The dashed red line represents the alarm threshold in Fig. 6(b). The PE divergence signal S_a was always above the threshold during the time interval $t \in [550, 850]$, which corresponded to the operating state switching phase. Next, the signal exceeded the threshold again at around $t = 1100s$; the corresponding qualitative trend d_x shown downward directions during $t \in [550, 1000]$ and $t \in [1100, 1500]$.

According to the reconstructed signals y in Fig. 7, the PE divergence signal S_a was only above the threshold during $t \in [550, 850]$. Meanwhile, both d_x and d_y shown downward directions during $t \in [550, 850]$. The trend

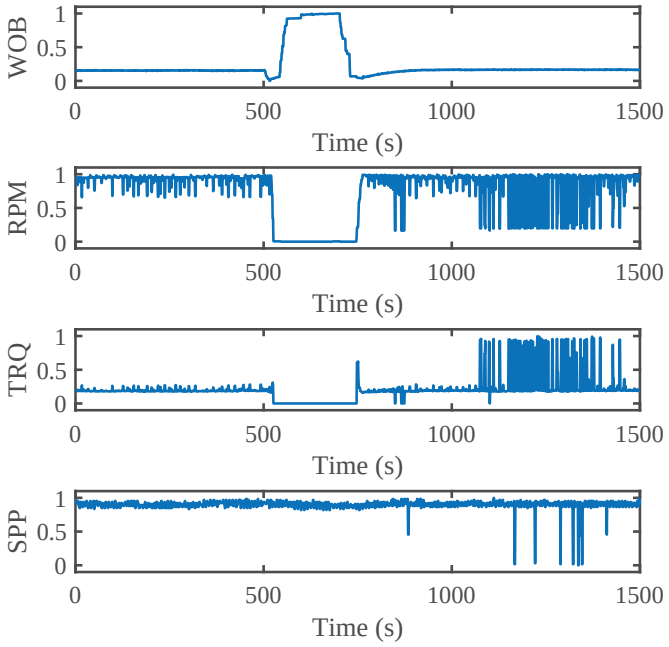

Figure 4: Case 1: Time series plots of original drilling signals.

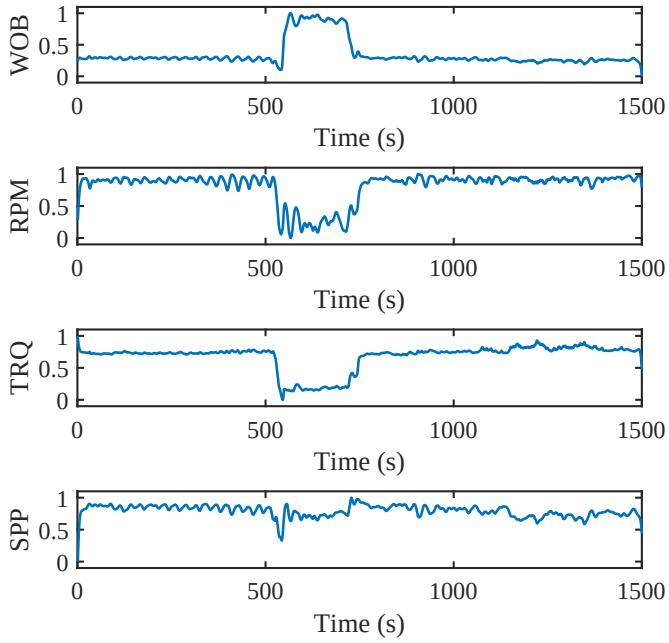

Figure 5: Case 1: Time series plots of reconstructed drilling signals.

of x was equal to that of y, indicating that the drilling system was in a normal condition, so the false alarm in $t \in [550, 850]$ was suppressed. However, the d_x exhibited downward directions in $t \in [1100, 1500]$, while the reconstructed d_y was quite stable. Since the change direction of d_y was inconsistent with that of d_x, the fault was detected in $t \in [1100, 1500]$. By checking d_x in Fig. 6 and d_y in Fig. 7, the alarm generation result is shown in Fig. 8, where 1 and 0 represent alarm and normal, respectively, and the red area indicates the faulty state.

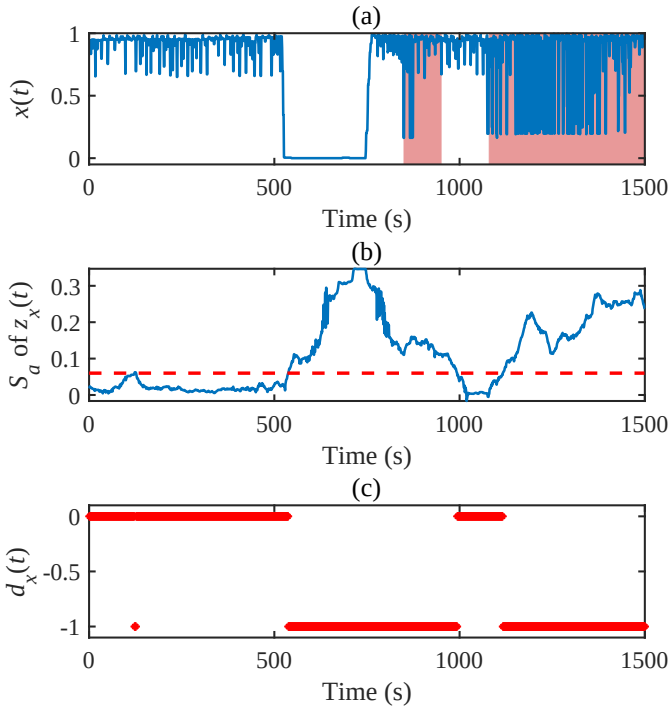

Figure 6: Case 1: Process monitoring results based on the original signal. (a): Time series plot of the original RPM signal x; (b): time series plot of the PE divergence S_a of the first derivative z_x; (c): time series plot of the corresponding qualitative trend d_x.

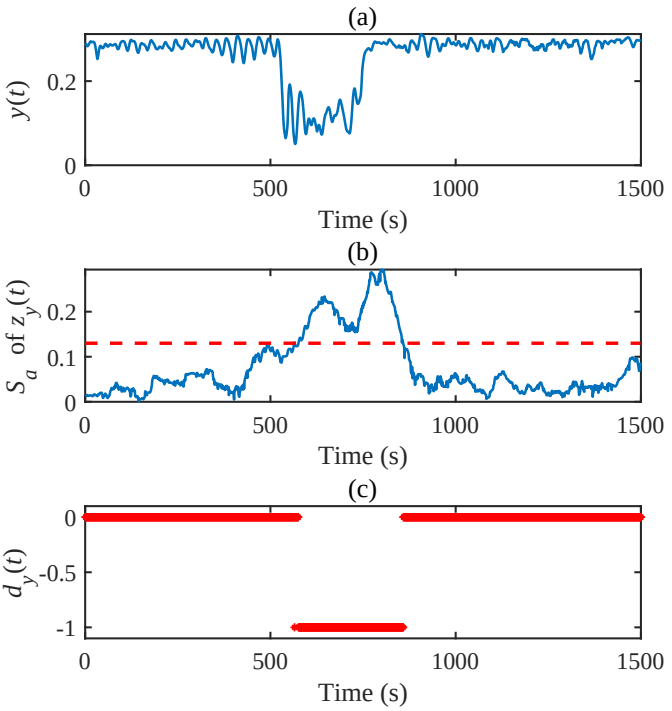

Figure 7: Case 1: Process monitoring results based on the reconstructed RPM signal.

The comparison experiment was conducted based on the 1500 samples. By comparing the actual label and alarm generation result, the FAR (F_A), MAR (M_A), and Accuracy (Acc) were utilized to evaluate the performance of these methods. The comparison results of different fault detection methods are shown in Table 1. The alarm threshold of the PCA-based method was determined based on normal historical data under a confidence level of 95%. The autoencoder model was trained based on normal historical data. The alarm threshold was determined based on the difference between the reconstructed and original signals under normal conditions. Compared with the proposed method, the fault detection strategy based on PE distance directly analyzes the original drilling process signal without extracting the qualitative trend. Since the drilling signals change significantly under both normal and faulty conditions, the traditional indicators failed to distinguish false alarms. The FAR of the proposed method was 8.48%, which was significantly lower than those of the T^2 of Principle Component Analysis (PCA), Autoencoder, and PE divergence. A convincing explanation for the method's superior performance is that normal change patterns are identified successfully using the reconstructed signals, thereby avoiding many false alarms.

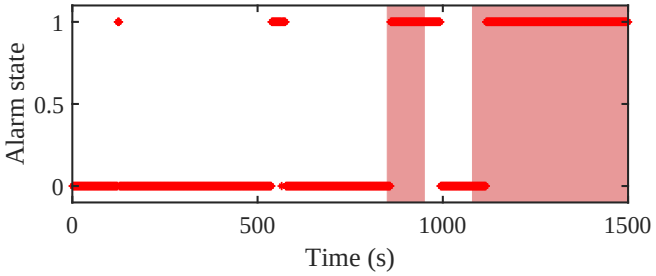

Figure 8: Process monitoring results in Case 1.

Table 1: Comparison results of different process monitoring methods for Case 1 (Ding, 2014; Hu et al., 2022b).

Method	F_A (%)	M_A (%)	Acc (%)
T^2 of PCA	32.41	8.81	75.80
Autoencoder	34.05	31.99	66.67
PE divergence	30.44	9.98	76.67
The proposed method	**8.48**	**8.45**	**91.53**

4.2. Case 2

In Case 2, time series plots of original drilling signals are shown in Fig. 9. The drilling system was operating normally until $t = 475s$. Then, the harsh geological environment led to a stuck pipe fault, causing fluctuations in TRQ and RPM signals in $t \in [475, 920]$. Finally, the drilling operator found the fault and adjusted the operating parameter at $t = 920s$, and the system returned to a normal steady state.

Fig. 10 shows the time series plots of the reconstructed signals calculated using the normal drilling behaviour model, whose inputs are original drilling signals in Fig. 9.

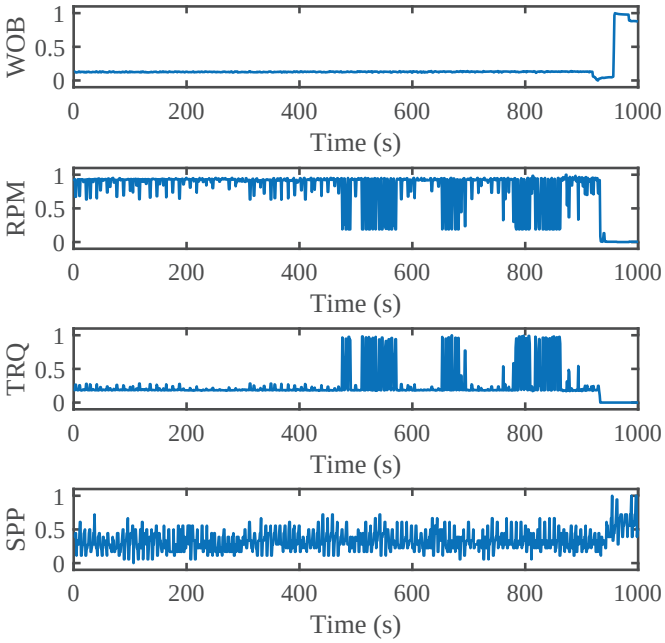

Figure 9: Case 2: Time series plots of original drilling signals.

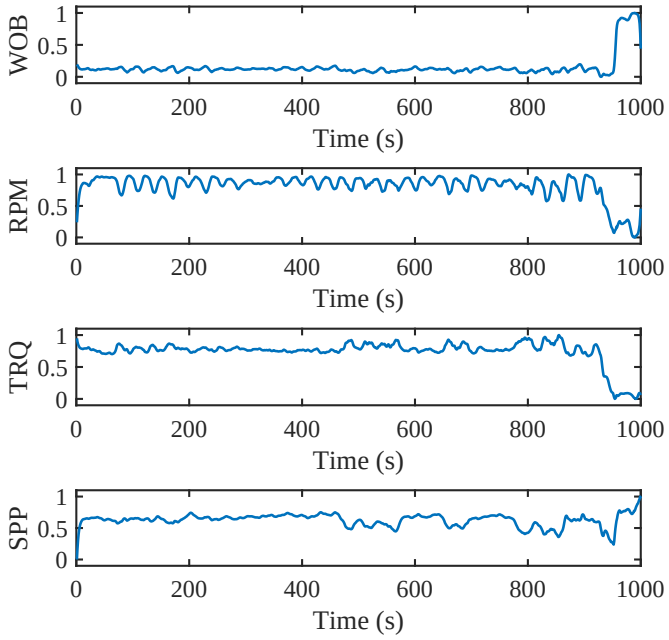

Figure 10: Case 2: Time series plots of reconstructed drilling signals.

It can be found that the original RPM and TRQ signals changed drastically in $t \in [480, 900]$, while the corresponding reconstructed signals showed no significant changes. Due to the adjustment of operating parameters, both the original and reconstructed signals changed sharply at $t = 920s$. Hence, the original and reconstructed signals exhibited similar trends, except that the original RPM and TRQ signals dropped significantly in $t \in [480, 900]$.

This case takes the TRQ signal as an example to illustrate the effectiveness of the proposed method. As shown

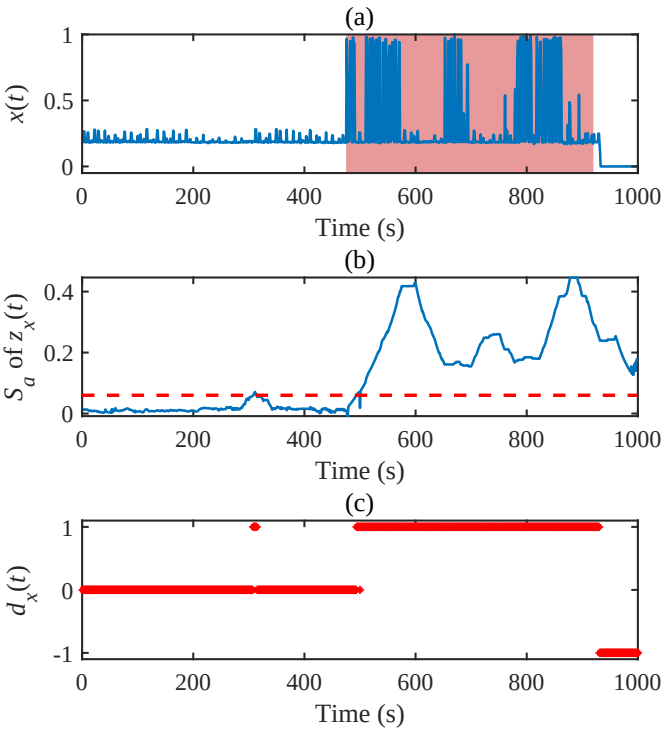

Figure 11: Case 2: Process monitoring results based on the normalized original TRQ signal.

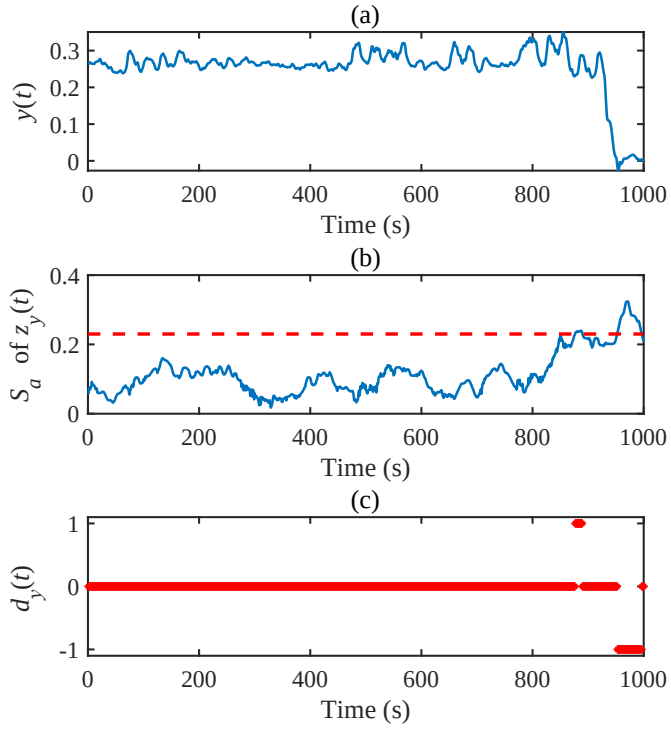

Figure 12: Case 2: Process monitoring results based on the reconstructed TRQ signal.

in Fig. 11, the original TRQ signal x climbed and fluctuated significantly from $t = 480s$, and then dropped to zero at $t = 920s$. This led to the PE divergence S_a of the

first derivative z_x exceeding the alarm threshold at around $t = 500s$. Consequently, the corresponding qualitative trend d_x shown an upward direction during $t \in [500, 920]$ and a downward direction during $t \in [920, 1000]$. Fig. 12 shows the time series plots of the reconstructed TRQ signal y, the PE divergence S_a of the first derivative z_y, and the corresponding qualitative trend d_y. The reconstructed signal was stable before $t = 920s$ and then dropped sharply. The PE divergence S_a was below the threshold before $t = 900s$, and then it climbed above the threshold until $t = 1000s$. As the PE divergence exceeded the threshold, the qualitative trend d_y changed from steady to downward direction at $t = 900s$.

According to Fig. 12(c), the d_y was in a steady state in $t \in [480, 920]$, which implies that d_x should not change significantly under normal conditions. However, a downhole fault led to abnormal changes in d_x, so it showed an upward direction in $t \in [480, 920]$. Hence, the fault was successfully detected in $t \in [480, 920]$. Subsequently, both d_x and d_y exhibited downward directions from $t = 920s$ due to changes in operating parameters. Although S_a signal was above the threshold in $t \in [920, 1000]$, the direction of d_x was consistent with that of d_y, so the false alarm was suppressed in $t \in [920, 1000]$. By checking d_x and d_y, the alarm generation result is concluded in Fig. 13.

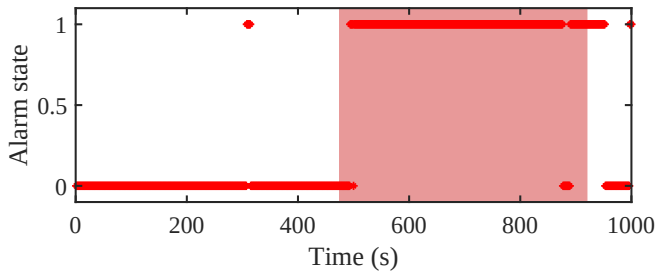

Figure 13: Process monitoring results in Case 2.

Table 2 gives the fault detection results using T^2 of PCA, Autoencoder, PE divergence, and the proposed method in terms of FAR, MAR, and accuracy. Since some dynamic changes under the normal condition were misclassified as faults, the FARs based on T^2 of PCA, Autoencoder, and PE divergence were 14.44%, 12.27%, and 12.03%, respectively. By contrast, the FAR of the proposed method was 1.35%, and the MAR was also lower than those of other methods. Hence, the proposed method exhibited an excellent fault detection ability and outperformed other methods.

4.3. Case 3

In this subsection, Case 3 is briefly described. The time series plots of original drilling signals and reconstructed signals are shown in Figs. 14 and 15, respectively. Downhole faults were found in $t \in [1400, 1500]$ and $t \in [1700, 2000]$. The RPM and TRQ signals changed drastically within the above intervals, while the corresponding reconstructed signals showed no significant changes.

Table 2: Comparison results of different process monitoring methods for Case 2 (Ding, 2014; Hu et al., 2022b).

Method	F_A (%)	M_A (%)	Acc (%)
T^2 of PCA	14.44	9.42	87.80
Autoencoder	12.27	25.78	81.70
PE divergence	12.03	13.85	87.11
The proposed method	**1.35**	**7.75**	**95.76**

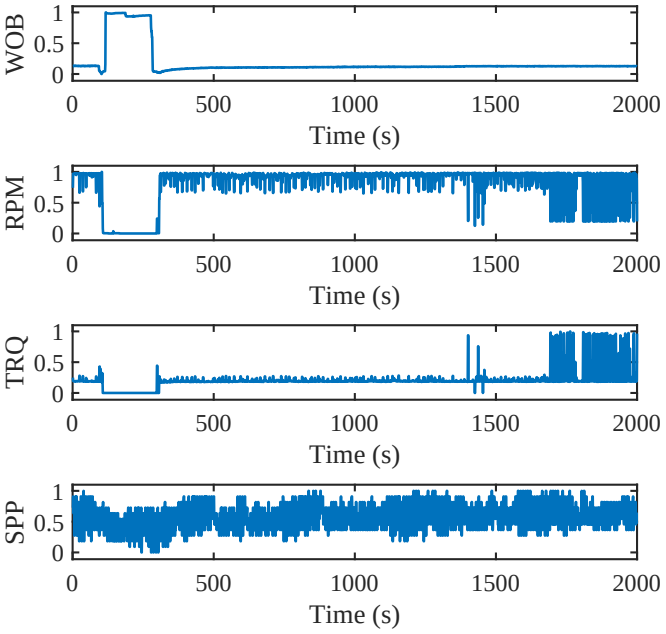

Figure 14: Case 3: Time series plots of original drilling signals.

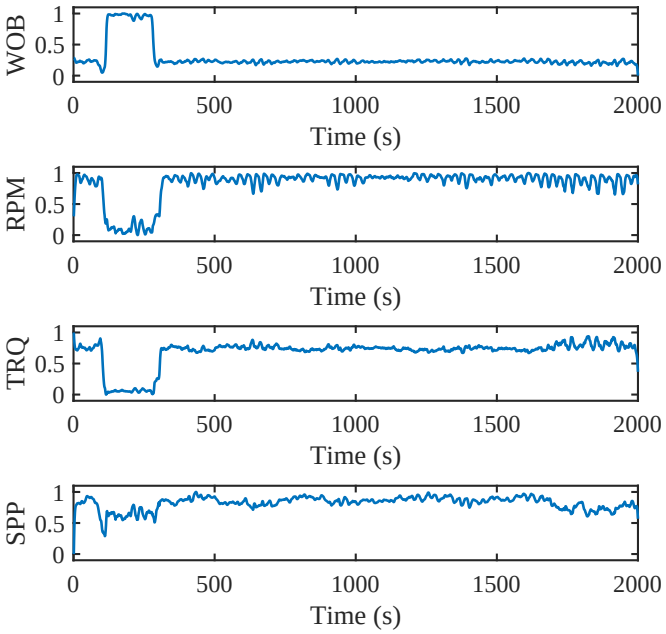

Figure 15: Case 3: Time series plots of reconstructed drilling signals.

Figs. 16 and 17 show the time series plots of the original and reconstructed RPM signals, the PE divergence of the first derivative, and the corresponding qualitative trend. As shown in Figs. 16(a) and 17(a), both the original RPM signal x and the corresponding reconstructed signal y exhibit downward step changes in $t \in [100, 300]$ due to a switching operation; then, the original signal x fluctuated significantly in $t \in [1400, 1500]$ and $t \in [1700, 2000]$, while the reconstructed signal was stable.

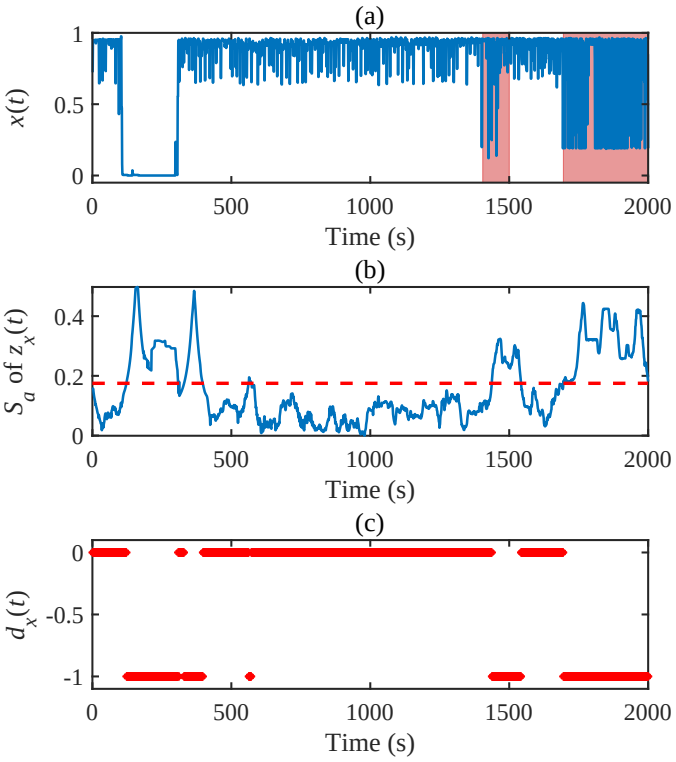

Figure 16: Process monitoring results based on the normalized original RPM signal in Case 3.

According to the extracted qualitative trends d_x and d_y in Figs. 16(c) and 17(c), the final alarm generation result is concluded in Fig. 18. It can be found that some false alarms in $t \in [100, 300]$ were suppressed, and the number of false alarms was reduced from 180 to 50. Subsequently, two faulty conditions were successfully detected in $t \in [1400, 1500]$ and $t \in [1700, 2000]$.

Table 3 gives the fault detection results using T^2 of PCA, Autoencoder, PE divergence, and the proposed method. Since the switching operation was misclassified as a fault, the FARs based on T^2 of PCA and Autoencoder were 19.27% and 26.91%, respectively. Compared with the proposed method, the PE distance method only used the original signal, and its FAR was 14.52%, which was higher than 8.57% of the proposed method. Meanwhile, the MAR of the proposed method was also lower than those of other methods. Hence, the proposed method outperformed other methods for drilling process monitoring.

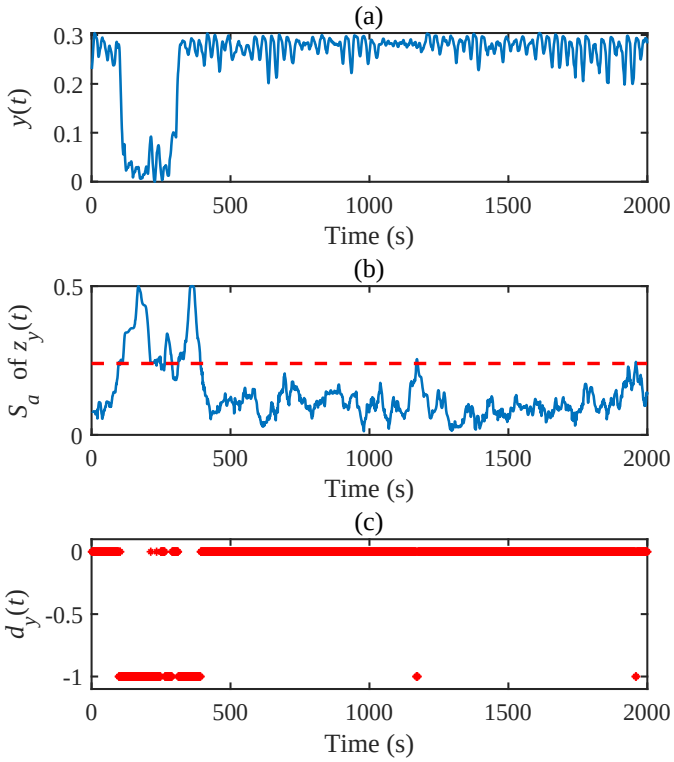

Figure 17: Process monitoring results based on the reconstructed RPM signal in Case 3.

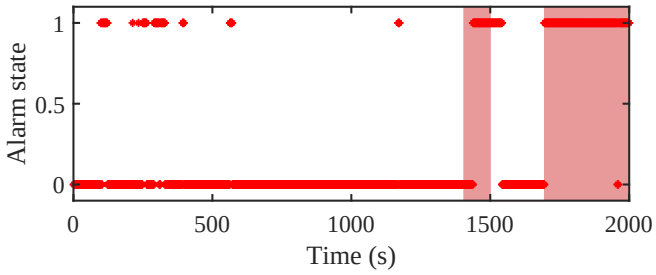

Figure 18: Process monitoring results in Case 3.

Table 3: Comparison results of different process monitoring methods for Case 3 (Ding, 2014; Hu et al., 2022b).

Method	F_A (%)	M_A (%)	Acc (%)
T^2 of PCA	19.27	30.35	78.50
Autoencoder	26.91	19.65	74.55
PE divergence	14.52	18.66	84.65
The proposed method	**8.57**	**8.73**	**91.40**

5. Conclusion

This work proposes a drilling process monitoring method using virtual sample generation and qualitative trend extraction to reduce false alarms. First, a data-driven reconstruction model describing the normal drilling behaviour is built to generate the expected healthy signal corresponding to the real-time collected signal. Next, a

change score is defined to determine the change points in real-time and expected healthy signals based on Pearson divergence and density ratio. Finally, the fault detection decision is made by checking the qualitative trend of the expected signal and that of the real-time signal to reduce the disturbance caused by stratigraphic uncertainty. Comparison results demonstrated that the proposed method outperformed the T^2 of PCA, Autoencoder, and PE divergence methods in most metrics. Especially in reducing false alarms under normal conditions, the proposed method shows apparent advantages. To sum up, this study contributes an effective way of reducing false alarms in geological drilling processes, and the proposed approach is promising for practical applications.

Besides the normal historical data, faulty data also contains valuable information for designing a drilling monitoring system. A critical issue to be further analyzed is improving the sensitivity of the algorithm to faulty data. A possible solution would be to introduce transfer learning methods or time series classification models like gated recurrent units to extract fault-related features from other drilling projects. Another future work will be concentrated on distinguishing many rising edges and one alarm for a long time. The above two alarm situations are quite different, and it is difficult to distinguish based on false alarm rates and accuracy.

Declaration of competing interest

The authors declare that they have no known competing financial interests or personal relationships that could have appeared to influence the work reported in this paper.

Acknowledgements

This work was supported by the National Natural Science Foundation of China under Grants 62173313, 61733016, 61903345, the Fundamental Research Funds for National Universities, China University of Geosciences (Wuhan), and the 111 project under Grant B17040.

References

Brodsky, E., Darkhovsky, B.S., 1993. Nonparametric methods in change point problems. volume 243. Springer Science & Business Media.

Chen, H., Jiang, B., Ding, S.X., Lu, N., Chen, W., 2019. Probability-relevant incipient fault detection and diagnosis methodology with applications to electric drive systems. IEEE Transactions on Control Systems Technology 27, 2766–2773.

Chen, H., Liu, H., Chu, X., Liu, Q., Xue, D., 2021. Anomaly detection and critical scada parameters identification for wind turbines based on LSTM-AE neural network. Renewable Energy 172, 829–840.

de Pater, I., Mitici, M., 2023. Developing health indicators and rul prognostics for systems with few failure instances and varying operating conditions using a LSTM autoencoder. Engineering Applications of Artificial Intelligence 117, 105582.

Ding, S.X., 2014. Data-driven design of fault diagnosis and fault-tolerant control systems. Springer.

Feng, L., Zhao, C., Huang, B., 2019. A slow independent component analysis algorithm for time series feature extraction with the concurrent consideration of high-order statistic and slowness. Journal of Process Control 84, 1–12.

Gonzalez, R., Huang, B., Lau, E., 2015. Process monitoring using kernel density estimation and bayesian networking with an industrial case study. ISA Transactions 58, 330–347.

Hu, J., Khan, F., Zhang, L., Tian, S., 2020. Data-driven early warning model for screenout scenarios in shale gas fracturing operation. Computers & Chemical Engineering 143, 107116.

Hu, W., Wang, J., Yang, F., Han, B., Wang, Z., 2022a. Analysis of time-varying cause-effect relations based on qualitative trends and change amplitudes. Computers & Chemical Engineering 162, 107813.

Hu, Z., Zhao, H., Peng, J., 2022b. Low-rank reconstruction-based autoencoder for robust fault detection. Control Engineering Practice 123, 105156.

Ji, H., Huang, K., Zhou, D., 2019. Incipient sensor fault isolation based on augmented mahalanobis distance. Control Engineering Practice 86, 144–154.

Jiang, H., Liu, G., Li, J., Zhang, T., Wang, C., 2020. Drilling fault classification based on pressure and flowrate responses via ensemble classifier in managed pressure drilling. Journal of Petroleum Science and Engineering 190, 107126.

Kamel, J.M., Yigit, A.S., 2014. Modeling and analysis of stick-slip and bit bounce in oil well drillstrings equipped with drag bits. Journal of Sound and Vibration 333, 6885–6899.

LeCun, Y., 1987. Phd thesis: Modeles connexionnistes de l'apprentissage (connectionist learning models).

Li, Y., Cao, W., Hu, W., Wu, M., 2021a. Abnormality detection for drilling processes based on Jensen-Shannon divergence and adaptive alarm limits. IEEE Transactions on Industrial Informatics 17, 6104–6113.

Li, Y., Cao, W., Hu, W., Wu, M., 2021b. Detection of downhole incidents for complex geological drilling processes using amplitude change detection and dynamic time warping. Journal of Process Control 102, 44–53.

Li, Y., Cao, W., Hu, W., Xiong, Y., Wu, M., 2021c. Incipient fault detection for geological drilling processes using multivariate generalized gaussian distributions and Kullback-Leibler divergence. Control Engineering Practice 117, 104937.

Liu, Q., Song, B., Ding, X., Qin, S.J., 2022. Fault diagnosis of dynamic processes with reconstruction and magnitude profile estimation for an industrial application. Control Engineering Practice 121, 105008.

Liu, S., Yamada, M., Collier, N., Sugiyama, M., 2013. Change-point detection in time-series data by relative density-ratio estimation. Neural Networks 43, 72–83.

Lu, C., Wu, M., Chen, L., Cao, W., 2021. An event-triggered approach to torsional vibration control of drill-string system using measurement-while-drilling data. Control Engineering Practice 106, 104668.

Nayeem, A.A., Venkatesan, R., Khan, F., 2016. Monitoring of downhole parameters for early kick detection. Journal of Loss Prevention in the Process Industries 40, 43–54.

Ni, Q., Ji, J., Feng, K., 2022. Data-driven prognostic scheme for bearings based on a novel health indicator and gated recurrent unit network. IEEE Transactions on Industrial Informatics , doi: 10.1109/TII.2022.3169465.

Sabah, M., Talebkeikhah, M., Agin, F., Talebkeikhah, F., Hasheminasab, E., 2019. Application of decision tree, artificial neural networks, and adaptive neuro-fuzzy inference system on predicting lost circulation: A case study from Marun oil field. Journal of Petroleum Science and Engineering 177, 236–249.

Sun, X., Sun, B., Zhang, S., Wang, Z., Gao, Y., Li, H., 2018. A new pattern recognition model for gas kick diagnosis in deepwater drilling. Journal of Petroleum Science and Engineering 167, 418–425.

Wang, C., Ma, J., Jin, H., Wang, G., Chen, C., Xia, Y., Gou, J., 2022. ACGAN and BN based method for downhole incident diagnosis during the drilling process with small sample data size.

Ocean Engineering 256, 111516.

Willersrud, A., Blanke, M., Imsland, L., Pavlov, A., 2015. Fault diagnosis of downhole drilling incidents using adaptive observers and statistical change detection. Journal of Process Control 30, 90–103.

Yamada, M., Suzuki, T., Kanamori, T., Hachiya, H., Sugiyama, M., 2013. Relative density-ratio estimation for robust distribution comparison. Neural Computation 25, 1324–1370.

Yang, H., Li, J., Liu, G., Wang, C., Jiang, H., Luo, K., Wang, B., 2019. A new method for early gas kick detection based on the consistencies and differences of bottomhole pressures at two measured points. Journal of Petroleum Science and Engineering 176, 1095–1105.

Zhang, J., Zhao, C., 2022. Condition-driven probabilistic adversarial autoencoder with nonlinear gaussian feature learning for nonstationary process monitoring. Journal of Process Control 117, 140–156.

Zhang, Y., Ren, Z., Zhou, S., Feng, K., Yu, K., Liu, Z., 2022. Supervised contrastive learning-based domain adaptation network for intelligent unsupervised fault diagnosis of rolling bearing. IEEE/ASME Transactions on Mechatronics , doi: 10.1109/TMECH.2022.3179289.

Zhang, Z., Lai, X., Wu, M., Chen, L., Lu, C., Du, S., 2021. Fault diagnosis based on feature clustering of time series data for loss and kick of drilling process. Journal of Process Control 102, 24–33.

Zhao, Y., Liu, S., Wang, Z., Ren, M., Sun, B., 2019. An adaptive pattern recognition method for early diagnosis of drillstring washout based on dynamic hydraulic model. Journal of Natural Gas Science and Engineering 70, 102947.

Zhou, Y., Chen, X., Wu, M., Cao, W., 2022. A novel modeling and drilling optimization method with suitable constraints in geological well. Control Engineering Practice 122, 105062.

Zhu, Q.X., Hou, K.R., Chen, Z.S., Gao, Z.S., Xu, Y., He, Y.L., 2021. Novel virtual sample generation using conditional GAN for developing soft sensor with small data. Engineering Applications of Artificial Intelligence 106, 104497.